Effect of an external field on capillary waves in a dipolar fluid

Jason P. Koski, Stan G. Moore, Gary S. Grest, and Mark J. Stevens

Effect of an external field on capillary waves in a dipolar fluid

Jason P. Koski,[*] Stan G. Moore, Gary S. Grest, and Mark J. Stevens

Sandia National Laboratories, Albuquerque, New Mexico 87185, USA

Abstract

The role of an external field on capillary waves at the liquid-vapor interface a dipolar fluid is investigated using molecular dynamics simulations. For fields parallel to the interface, the interfacial width squared increases linearly with respect to the logarithm of the size of the interface across all field strengths tested. The value of the slope decreases with increasing field strength indicating that the field dampens the capillary waves. With the inclusion of the parallel field, the surface stiffness increases with increasing field strength faster than the surface tension. For fields perpendicular to the interface, the interfacial width squared is linear with respect to the logarithm of the size of the interface for small field strengths and the surface stiffness is less than the surface tension. Above a critical field strength that decreases as the size of the interface increases, the interface becomes unstable due to the increased amplitude of the capillary waves.

---
[*] jkoski@sandia.gov

I. INTRODUCTION

An intrinsic aspect of liquid-vapor systems is the presence of Goldstone fluctuations or "capillary waves" at the interface [1, 2]. For simple fluids without an external field, the amplitude of the capillary waves is due to a balance between thermal fluctuations and surface tension[3, 4]. This energetic balance results in the interfacial width squared Δ^2 increasing logarithmically with increasing interfacial length L, where Δ^2 is a measure of the capillary waves amplitude. In dipolar fluids, the introduction of an external field introduces new effects on the interfacial structure and a description of the capillary waves becomes more complex. An external field on a dipolar fluid results in an anisotropic fluid for which capillary wave theory requires the inclusion of the surface stiffness instead of the surface tension[5–8]. The surface stiffness arises in the Taylor series expansion of the surface tension as a function of surface roughness. The capillary wave theory for anisotropic fluid remains similar to simple fluids but with the surface stiffness replacing the surface tension.

While the effect of an external field on fluids is fundamentally important, theoretical treatment of interfaces in a field have received only limited attention with almost no work on capillary waves[9–13]. This is despite the importance of capillary waves in the nanoscale structure of interfaces [14–17]. A relation between the amplitude of the capillary waves, the field strength, and surface stiffness is lacking and measuring these quantities experimentally is difficult, which makes developing an empirical relation among these quantities a challenge. To overcome this, we perform molecular dynamics (MD) simulations to examine the effect of an external field on the capillary waves in a simple dipolar fluid and investigate the corresponding dependence of both the surface tension and surface stiffness on the direction and amplitude of an external field. The dipolar system we treat can be considered either electric of magnetic, and our results apply to both systems so long as a purely dipolar model applies.

Dipolar fluids are an important class of fluids in that an external field can be used as an additional parameter to control the structure of the fluid. While the interfacial structure, phase transitions and normal field instability for dipolar fluids in a field has been studied both experimentally[18–20, 27] and theoretically [9, 12, 21–26, 28–35], a description of the capillary waves' role in these topics is lacking. Though progress has been made using density functional theory (DFT) of simple fluids to provide a connection between the Hamiltonian of the system and standard capillary wave theory [36–38], describing the surface tension in the presence of a field and its relation to the

capillary waves remains non-trivial. As mentioned previously, this becomes even more complex for a dipolar fluid in a field, where the surface stiffness is necessary to describe the capillary waves and no longer reduces to the surface tension.
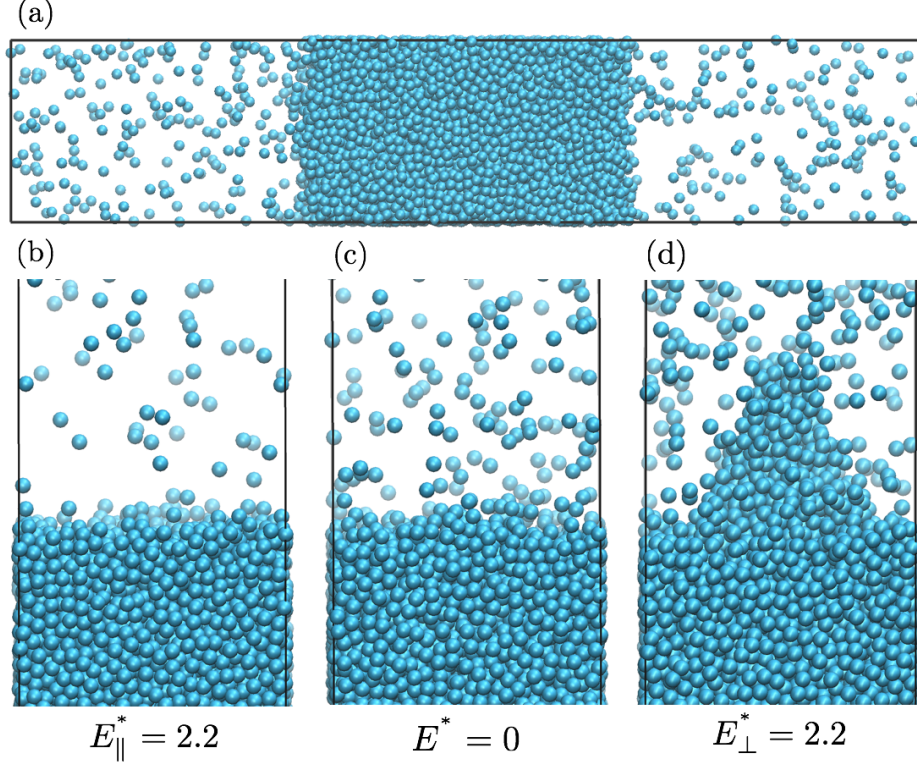
(a)

(b)   (c)   (d)

$$E_{\parallel}^* = 2.2 \qquad E^* = 0 \qquad E_{\perp}^* = 2.2$$

Figure 1. (a) Snapshot of the Stockmayer liquid-vapor system with $E^* = 0$. Zoomed-in snapshots of the liquid-vapor interface with (b) $E_{\parallel}^* = 2.2$, (c) $E^* = 0$, and (d) $E_{\perp}^* = 2.2$. $L^* = 20$ in all snapshots.

In contrast to theoretical and experimental approaches, molecular simulations of simple fluids provide a straightforward method to describe the relation of the surface tension and capillary waves with direct determination of interface structure and the surface tension. Previous simulation work for both Lennard-Jones systems and atomistic water without an external field have shown that the surface tension determined from the amplitude of the logarithmic divergence of the capillary interfacial width agrees with the thermodynamically calculated surface tension [3, 4]. In this work however, we find that an external field acting on a dipolar fluid alters the basic relation connecting the capillary interfacial width and surface tension as the surface tension is no longer equal to the surface stiffness. From these simulations, we are able to assess trends in the surface stiffness as a function of external field strength and their relation to the capillary waves. Specifically, the effect on the capillary waves depends strongly on the field direction relative to the interface as illustrated

3

in Fig 1. For fields parallel to the interface, the amplitude of the capillary waves are reduced much more than one would predict from the small increase in surface tension with increasing field strength. While in a perpendicular field, the capillary waves are enhanced for weak fields until they become unstable at a critical field strength[9, 39].

II. MODEL AND METHODS

Here we study the prototypical dipolar system, the Stockmayer fluid, which is described by Lennard-Jones (LJ) particles with fixed-point dipoles [40]. The LJ potential is

$$U_{LJ}(r) = 4\varepsilon \left[\left(\frac{\sigma}{\mathbf{r}_{ij}} \right)^{12} - \left(\frac{\sigma}{\mathbf{r}_{ij}} \right)^6 \right],\tag{1}$$

where σ is the LJ diameter, ε is the LJ energy parameter and $r_{ij} = |\mathbf{r}_i - \mathbf{r}_j|$ is the interparticle distance between particles i and j. The dipolar pair potential is given by

$$U_{dipole}(r) = \frac{\mu_i \cdot \mu_j}{\mathbf{r}_{ij}^3} - 3 \frac{(\mu_i \cdot \mathbf{r}_{ij})(\mu_j \cdot \mathbf{r}_{ij})}{\mathbf{r}_{ij}^5}\tag{2}$$

and the interaction of the dipole with the external field is $-\mu_\mathbf{i} \cdot \mathbf{E}$, where μ_i is the point dipole of particle i and $\mathbf{E}$ is the external field. As the field is uniform, there is no net force acting on the dipoles. The external field induces a torque on the dipoles, which influences the dipoles to orient with the field [35].

We use reduced LJ units throughout this work, which we denote with a superscript asterisk. The LJ reduced temperature, $T^* = T/(\varepsilon/k_B)$, and reduced dipole moment, $\mu^* = \mu/\sqrt{\varepsilon\sigma^3}$, were each set equal to 1 in all simulations. The LJ reduced surface tension and surface stiffness are $\gamma^* = \gamma/(\varepsilon/\sigma^2)$ and $\kappa^* = \kappa/(\varepsilon/\sigma^2)$, respectively. The reduced electric field is $E^* = E\sqrt{\sigma^3/\varepsilon}$, which we apply either parallel ($E_\parallel$) or perpendicular ($E_\perp$) to the interface. The long-range dipole interaction was treated using a lattice Ewald sum with tinfoil boundary conditions and a 2D slab correction [35]. In this work, the LJ dispersion ($\mathbf{r}^{-6}$) interaction is also treated using an Ewald sum with a real-space cutoff of $r_c = 7.5\sigma$, which eliminates effects of a finite cutoff on the liquid-vapor coexistence curve and on the interfacial properties. Full details of the simulation method and results for the liquid-vapor coexistence curve in the presence of an external field can be found in ref. [35]. In this previous work it was shown that the critical temperature for $E^* = 0$ and $\mu^* = 1$ is $T_c^* = 1.415$. Moreover, the addition of a field parallel to the interface increases T_c^* while fields perpendicular to the interface reduce T_c^*. For example, with $\mu^* = 1$, $T_c^* = 1.423$ for $E_\parallel^* = 2.0$

while $T_c^* = 1.352$ for $E_\perp = 2.0$. Therefore, $T^* = 1$ is sufficiently far from the critical temperature even in the presence of strong external fields. There is no significant ordering in the liquid phase in the absence of a field for $T^* = 1$ [35].

To study the dependence of the amplitude of the capillary waves on the interfacial area of the liquid-vapor interface, we vary the length of the simulation cell parallel to the interface, $L_x = L_y = L$. The length of the simulation cell perpendicular to the interface was held constant at $L_z^* = 100$. A snapshot of the liquid-vapor system for $L^* = 20$ and $E^* = 0$ is shown in Fig. 1a. For $L^* = 10$, the number of particles was $N = 2610$ and N increases linearly with interfacial area. The largest system studied, $L^* = 80$ contained $N = 167,040$ particles. Larger systems were computationally prohibitive due to the large number of particles and expense of the Ewald summation. For each value of L, that system was equilibrated at zero field for 2000τ, where $\tau = \sigma\sqrt{(m/\varepsilon)}$ is the LJ unit of time and m is the mass of a particle. The simulations were then run for an additional $10,000\tau$ for $L \le 40$ and an additional 4000τ for $L > 40$.

The surface tension is calculated as the integral difference between the components of the pressure tensor that are normal and tangential to the interface $P_\perp(z)$ and $P_\parallel(z)$,

$$\gamma = \frac{1}{2} \int_{-\infty}^{\infty} dz \left(P_\perp(z) - P_\parallel(z) \right). \tag{3}$$

For the geometry of our system (shown in Fig. 1a), the diagonal components of the pressure tensor $\mathbf{P}$ can be used to calculate the surface tension,

$$\gamma = \frac{L_z}{2} \left[\langle P_{zz} \rangle - \left(\langle P_{xx} \rangle + \langle P_{yy} \rangle \right)/2 \right], \tag{4}$$

where the interface is normal to the z-direction and the factor of 1/2 accounts for the two interfaces. The components of the pressure tensor are calculated every 0.1τ and averaged over the entire run. In the absence of an external field, a second method to calculate the surface tension is from the amplitude of the logarithmic divergence of the interfacial width [1, 2, 41]. The root of this derivation is is based on the increase in the surface area of the interface due to fluctuations. Accordingly, the Hamiltonian of the interface is a product of the surface tension and the interfacial area defined by

$$\mathcal{H}(z_0) = \gamma \int dx\, dy \left[\sqrt{1 + \left(\frac{\partial z_0}{\partial x}\right)^2 + \left(\frac{\partial z_0}{\partial y}\right)^2} - 1 \right], \tag{5}$$

$$\approx \frac{\gamma}{2} \int dx\, dy |\nabla z_0(x,y)|^2 \tag{6}$$

5

where $z_0(x, y)$ is the mean location of the interface in the z-direction. Rewriting Eq. 6 in Fourier space, the Hamiltonian is now given by

$$\mathscr{H}(z_0) \approx \frac{\gamma}{2} \int d\mathbf{q}\, \mathbf{q}^2 |z_0(\mathbf{q})|^2, \tag{7}$$

where $\mathbf{q}$ is the two-dimensional vector in Fourier space. The mean-square amplitude for each excitation mode of the interface is given by

$$\langle |z_0(\mathbf{q})|^2 \rangle = \frac{k_B T}{4\pi^2 \gamma \mathbf{q}^2} \tag{8}$$

due to the equipartition theorem. Taking the integral over all possible wavelengths $\mathbf{q}$, results in

$$\langle |z_0|^2 \rangle = \frac{k_B T}{4\pi^2 \gamma} \int_{\mathbf{q}_{min}}^{\mathbf{q}_{max}} \frac{d\mathbf{q}}{\mathbf{q}^2}, \tag{9}$$

$$= \frac{k_B T}{2\pi\gamma} \ln\left(\frac{L}{B_0}\right), \tag{10}$$

where $\mathbf{q}_{min} = 2\pi/L$, $\mathbf{q}_{max} = 2\pi/B_0$, and B_0 is a characteristic short distance cutoff. Equation 10 represents the broadening of the interfacial width due to capillary wave fluctuations. If it is assumed that the capillary wave fluctuations are decoupled from the intrinsic interfacial width, the total interfacial width can be written as

$$\Delta^2 = \Delta_0^2 + \frac{k_B T}{2\pi\gamma} \ln\left(\frac{L}{B_0}\right), \tag{11}$$

where Δ_0^2 is the intrinsic interfacial width.

However, with the inclusion of an external field the order in both the vapor and liquid phases are no longer isotropic[5]. This leads to the emergence of the surface stiffness defined by

$$\kappa = \gamma \Big|_{\theta=0} + \frac{d^2\gamma}{d\theta^2} \Big|_{\theta=0}, \tag{12}$$

where θ is the inclination angle defined with respect to the plane of the interface. If we assume the electric field contribution to the interfacial Hamiltonian is embedded into the surface stiffness, γ is simply replaced by κ in Eqs. 5 -11 such that the total interfacial width is now given by

$$\Delta^2 = \Delta_0^2 + \frac{k_B T}{2\pi\kappa} \ln\left(\frac{L}{B_0}\right), \tag{13}$$

To calculate Δ, the density profile through the interface was averaged over the x-y plane, $\rho(z)$, and fit to an error function $\mathrm{erf}[z/(\Delta\sqrt{2})]$. Previous work has shown that for an LJ fluid with no external field, κ reduces to γ [3].

6

III. RESULTS AND DISCUSSION

Previously, we showed that the structural order in the dipoles in the two phases is different and depends on the field direction [35]. Related is the different boundary conditions for the parallel and perpendicular fields at the liquid-vapor interface because of the dielectric discontinuity there. For the vapor phase, the order parameter $\alpha = \langle \cos \theta \rangle$, where $\cos \theta = \hat{\mu} \cdot \hat{\mathbf{E}}$, is the same for either field direction. At $E^* = 1.0$, $\mu^* = 1.0$ and $T^* = 1.0$, α is about 0.3 for the vapor phase. For the field parallel to the interface, α is larger in the liquid phase (0.54 for the case given above). In contrast, α is smaller for the field perpendicular (0.09 for the same case). These liquid values are related to the boundary conditions. For the parallel direction, the field is continuous and α has the same value as the bulk liquid at the same E^*. For the perpendicular direction, the displacement field is continuous and α has the same value as the bulk liquid at the same E^*/ε.

We first consider the parallel field case. Figure 2a shows Δ^2 as a function of $\ln(L^*)$ for varying values of $E_\parallel^*$ where the error bars are the standard deviation of Δ^2. Interestingly, Δ^2 increases linearly with $\ln(L^*)$ across a large range of $E_\parallel^*$ as shown by the linear fits to the data. From these trends, we can conclude that the logarithmic dependence shown in Eqs. 11 and 13 still occurs in a parallel field and that any nonlogarithmic corrections from the field are negligible. However, the external field has a strong effect on the amplitude of $\ln(L^*)$ with respect to Δ^2. From the data in Fig. 2a, we find the amplitude of the logarithmic term given by the slope of the fit lines decreases with increasing $E_\parallel^*$ as shown in Fig. 2b. The inset of Fig. 2b shows that at very high $E_\parallel^*$ the slope becomes nearly flat and the slope's dependence on $E_\parallel^*$ plateaus. While we can analyze the trend in the slope of Δ^2 as a function of $\ln(L^*)$, decoupling the dependence of the external field strength is a non-trivial task without a theoretical basis for its functional form. However, using Eq. 4 to determine γ and Eq. 13 to determine κ, we find the difference between κ and γ increases with increasing $E_\parallel^*$ as shown in Fig 2c. The dominant effect in the change of the surface tension as a function of the external field is a result of the external field affecting the dipole-dipole interaction described by Eq. 2. Thus, Fig. 2c demonstrates that the reduction of the capillary waves with $E_\parallel^*$ is not solely a result of the increase in the surface tension.

While fields parallel to the interface reduce fluctuations in the interfacial width, fields perpendicular to the interface have the opposite effect. In contrast to the parallel field case, the surface tension decreases with $E_\perp^*$ and $\gamma^* > \kappa^*$. Similar to the parallel field case, the difference between γ^* and κ^* becomes larger with field strength. For small $E_\perp^*$, the interfacial width can be calculated
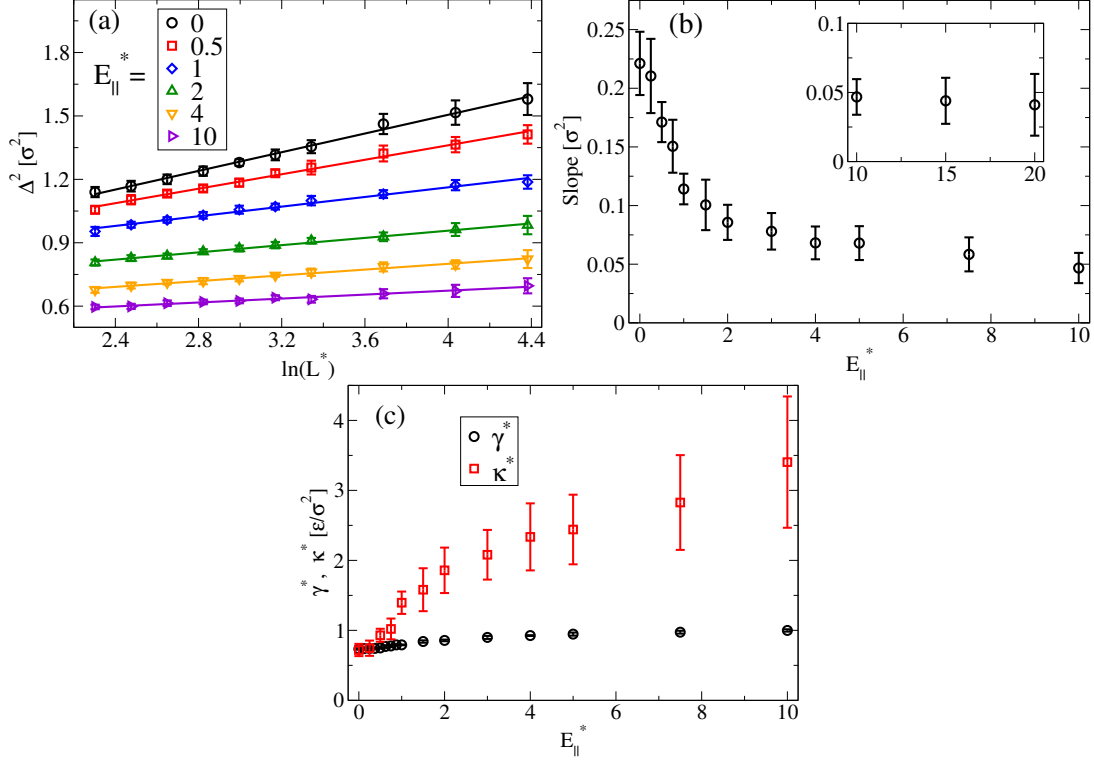
Figure 2. (a) Interfacial width squared Δ^2 as a function $\ln(L^*)$ for varying external field strengths applied parallel to the interface, $E_\parallel^*$ for $E_\parallel^*$ values where $E_\parallel^* = 0$ (black circles), $E_\parallel^* = 0.5$ (red squares), $E_\parallel^* = 1$ (blue diamonds), $E_\parallel^* = 2$ (green upward triangles), $E_\parallel^* = 4$ (orange downward triangles), and $E_\parallel^* = 10$ (sideways triangles). The lines are linear fits of the data. (b) Slope of Δ^2 vs. $\ln(L^*)$ as a function of $E_\parallel^*$. The inset emphasizes the plateau of the slope at very high $E_\parallel$ values. (c) γ^* (black circles) and κ^* (red squares) as a function of $E_\parallel^*$.

and examined as a function of $E_\perp^*$. Fig. 3 shows the interfacial width increases linearly with $\ln(L^*)$ for $E_\perp^* = 0$ and 0.5. However, the linear relation breaks down for large $E_\perp^*$ and large L^*. Figure 3 shows deviations from the linear dependence in Δ^2 for $E_\perp^* = 1.0$ for large L^*. The deviation is an indication of the onset of an instability. This analysis was not done for larger $E_\perp^*$ because of this instability. The perpendicular field orients the dipoles at the interface perpendicular to the interface, which cluster together and form protrusions as shown in Figure 1d.

The emergence of these protrusions depends on both $E_\perp^*$ and L^*. Figure 4 shows visualizations for varying $E_\perp^*$ and L^* at $t = 10,000\tau$. For $E_\perp^* = 1.0$, large protrusions are not visible for $L^* \leq 40$. Increasing the field to $E_\perp^* = 1.6$ results in clear protrusions appearing at $L^* = 40$, while the interfaces remain smooth for $L^* = 20$. Increasing $E_\perp^*$ even further to 2.2, protrusions now
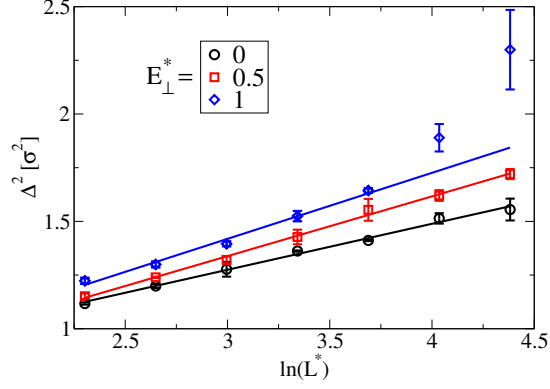
Figure 3. Interfacial width squared as a function of $\ln(L^*)$ for varying $E_\perp^*$ for $E_\perp^* = 0$ (black circles), $E_\perp^* = 0.5$ (red squares), $E_\perp^* = 1$ (blue diamonds). The lines are linear fits to the data. For $E_\perp^* = 1$, the solid line is a linear fit for $L^* \leq 40$.

occurs for $L^* = 20$. A complete instability appears at $E_\perp^* = 2.2$ for $L^* = 40$, where the interfaces completely rearrange so that they are parallel to the field. The trends in Fig. 4 demonstrate that above a critical value in $E_\perp^*$, the interface becomes unstable.
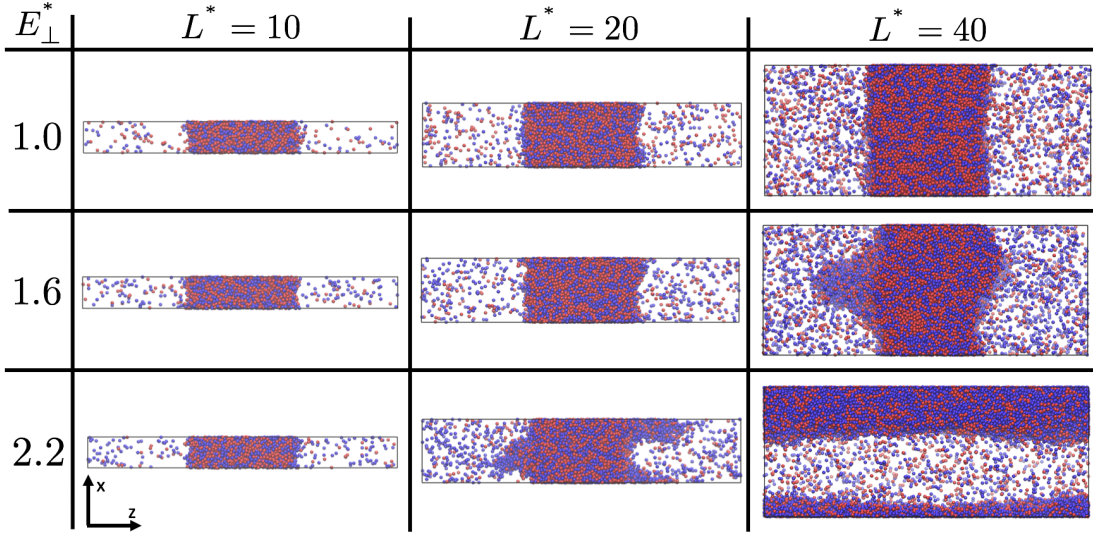

Figure 4. Visualization of dipolar liquid-vapor system for varying $E_\perp^*$ and L^* values. Each snapshot is at $t = 10,000\tau$. Every atom is colored red or blue if $\cos\theta$ is below or above 0.3, respectively, where θ is the angle between the dipole moment and the z-axis. $\cos\theta = 1$ means the dipole is aligned parallel with the field while $\cos\theta = 0$ means the dipole is aligned perpendicular to the field

An estimate of the critical value of $E_\perp^*$ where the onset of protrusions occur as a function of L^* is shown in Fig. 5. We define the interface to be unstable when the interface shows notable

protrusions after $t = 4000\tau$ (e.g. Fig. 4 at $L^* = 20$ and $E_\perp^* = 2.2$) whereas the interface is stable if the protrusions are absent (e.g. $L^* = 10$ in Fig. 4). Based on these definitions, an approximate (upper bound) phase boundary has been determined for the critical $E_\perp^*$ as a function of L^*. Figure 5 shows that the critical $E_\perp^*$ decreases as L^* increases. For larger L^*, protrusions with larger wavelengths are possible, lowering the critical value of $E_\perp^*$. These results suggest an alternative method to determine the critical $E_\perp^*$ rather than by using the point where the deviation from linearity of Δ^2 vs. $\ln(L^*)$ occurs (Fig. 3). In the more quantitative analysis of Fig. 3, the critical value in $E_\perp^* \approx 1.0$ for $L^* = 40\sqrt{2}$ while from visual inspection (Fig. 5), $E_\perp^* \approx 1.3$. The visual method requires much less data as a function of L^* and gives similar results.
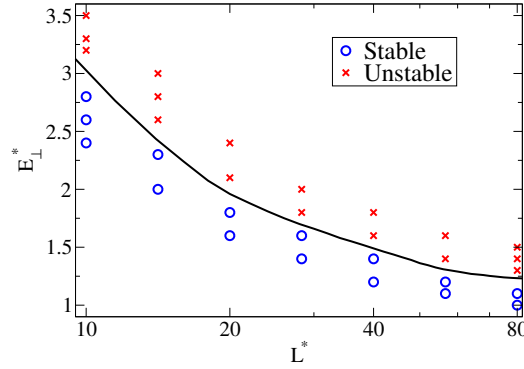

Figure 5. Stability map of liquid-vapor phase for external electric field applied perpendicular to the interface, $E_\perp^*$, as a function of the interface length, L^*. The red x's and blue circles denote unstable and stable state points, respectively. The black line is an approximate phase boundary of the critical value of $E_\perp^*$ as a function of L^*.

In conclusion, we have examined capillary waves at the liquid-vapor interface for a prototypical dipolar system, the Stockmayer fluid, in an external field. The addition of an external field requires a description in terms of the surface stiffness rather than the surface tension to describe the amplitude of the capillary waves. Both the surface stiffness and the capillary waves depends strongly on the field direction, parallel vs. perpendicular. When the field is parallel to the interface, the width of the interface decreases and both the surface stiffness and surface tension increases. However, the surface stiffness increases much faster with increasing field strength than the surface tension. This results in a strong reduction of the capillary waves. The behavior for the perpendicular external field is fundamentally different. Not only does the interfacial width increase, but the system becomes unstable for sufficiently large field strength. At increasingly high field strengths, the interface reorients parallel to the field direction for the liquid film thickness studied in the sim-

ulations. Overall, this work provides new results to be verified experimentally and provides a new relation to be derived theoretically.

[1] F. P. Buff, R. A. Lovett, and F. H. Stillinger, Phys. Rev. Lett. **15**, 621 (1965).

[2] J. Rowlinson and B. Widom, *Molecular Theory of Capillary* (Clarendon Press, Oxford, 1982).

[3] S. W. Sides, G. S. Grest, and M.-D. Lacasse, Phys. Rev. E **60**, 6708 (1999).

[4] A. E. Ismail, G. S. Grest, and M. J. Stevens, J. Chem. Phys. **125**, 014702 (2006).

[5] V. Privman, International Journal of Modern Physics C **3**, 857 (1992).

[6] M. Hasenbusch and K. Pinn, Physica A: Statistical Mechanics and its Applications **192**, 342 (1993).

[7] P. Nozieres and F. Gallet, Journal de Physique **48**, 353 (1987).

[8] B. J. Block, S. Kim, P. Virnau, and K. Binder, Physical Review E **90**, 062106 (2014).

[9] Y. Tsori, Rev. Mod. Phys. **81**, 1471 (2009).

[10] R. Rodriguez and P. R. Antoniewicz, Chem. Phys. Lett. **66**, 400 (1979).

[11] J. Goodisman, J. Phys. Chem. **96**, 6355 (1991).

[12] K. J. Schweighofer and I. Benjamin, J. Electroanalytical Chemistry **391**, 1 (1995).

[13] L. Daikhin, A. Kornyshev, and M. Urbakh, J. Electroanalytical Chemistry **483**, 68 (2000).

[14] M. Fukuto, B. M. Ocko, D. J. Bonthuis, R. R. Netz, H.-G. Steinrück, D. Pontoni, I. Kuzmenko, J. Haddad, and M. Deutsch, Phys. Rev. Lett. **117**, 256102 (2016).

[15] M. K. Sanyal, S. K. Sinha, K. G. Huang, and B. M. Ocko, Phys. Rev. Lett. **66**, 628 (1991).

[16] J. Daillant and M. Alba, Reports Prog. Phys. **63**, 1725 (2000).

[17] J. S. Huang and W. W. Webb, J. Chem. Phys. **50**, 3677 (1969).

[18] P. Debye and K. Kleboth, J. Chem. Phys. **42**, 3155 (1965).

[19] D. Beaglehole, J. Chem. Phys. **74**, 5251 (1981).

[20] J. Hegseth and K. Amara, Phys. Rev. Lett. **93**, 057402 (2004).

[21] P. Teixeira and M. T. da Gama, J. Phys.: Cond. Matt. **3**, 111 (1991).

[22] M. Van Leeuwen, B. Smit, and E. Hendriks, Mol. Phys. **78**, 271 (1993).

[23] M. J. Stevens and G. S. Grest, Phys. Rev. E **51**, 5976 (1995).

[24] A. Onuki, Physica A: Statistical Mechanics and its Applications **217**, 38 (1995).

[25] K. Kiyohara, K. E. Gubbins, and A. Z. Panagiotopoulos, J. Chem. Phys. **106**, 3338 (1997).

[26] K. Kiyohara, K. J. Oh, X. C. Zeng, and K. Ohta, Mol. Simulat. **23**, 95 (1999).

[27] E. Schäffer, T. Thurn-Albrecht, T. P. Russell, and U. Steiner, Europhys. Lett. **53**, 518 (2001).

[28] V. Warshavsky, T. Bykov, and X. C. Zeng, J. Chem. Phys. **114**, 504 (2001).

[29] V. B. Warshavsky and X. C. Zeng, Phys. Rev. E **68**, 051203 (2003).

[30] J. Dudowicz, K. F. Freed, and J. F. Douglas, Phys. Rev. Lett. **92**, 045502 (2004).

[31] I. Szalai and S. Dietrich, J. Phys.: Condens. Matter **20**, 204122 (2008).

[32] R. Jia and R. Hentschke, Phys. Rev. E **80**, 051502 (2009).

[33] S. Stepanow and T. Thurn-Albrecht, Phys. Rev. E **79**, 041104 (2009).

[34] S. Samin and Y. Tsori, J. Phys. Chem. B **115**, 75 (2011).

[35] S. G. Moore, M. J. Stevens, and G. S. Grest, Phys. Rev. E **91**, 022309 (2015).

[36] K. R. Mecke and S. Dietrich, Phys. Rev. E **59**, 6766 (1999).

[37] E. Chacón and P. Tarazona, J. Phys.: Cond. Matt. **28**, 244014 (2016).

[38] A. Parry, C. Rascón, and R. Evans, J. Phys.: Cond. Matt. **28**, 244013 (2016).

[39] M. D. Cowley and R. E. Rosensweig, J. Fluid Mech. **30**, 671 (1967).

[40] W. H. Stockmayer, J. Chem. Phys. **9**, 398 (1941).

[41] M.-D. Lacasse, G. S. Grest, and A. J. Levine, Phys. Rev. Lett. **80**, 309 (1998).